An Evapotranspiration formulation from the Relative Surface Moisture

DANIELA GIROLIMETTO[*§] AND VIRGINIA VENTURINI[§]

[§] Centro de Estudios Hidro Ambientales - Facultad de Ingeniería y Ciencias Hídricas, Universidad Nacional del Litoral, C.C. 217, Santa Fe, 3000. Argentina.

*Corresponding author. Email: dgirolimetto@fich.unl.edu.ar

Abstract

The agriculture water consumption is about 60 - 70% of the total water withdrawals, thus its computations and intelligent use is the key of success of any water management plan. In recent decades the scientific community has developed a wide range of models to calculate evapotranspiration (ET) based on remote sensing information. The method developed by Venturini et al., (2008) computes ET based on a new parameter (T_u) which depends on surface temperature (T_s) and the surface moisture content. The original T_u estimations do not represent the physics of the problem and needed further analysis. Here, a modified methodology to estimate the main parameter of Venturini et al. method is presented. The new formulation relates the short wave infrared (SWIR) properties to the relative surface moisture. The new method for estimating T_u, significantly improves the original Venturini et al. Our results yield a root mean squared error (RMSE) of about 11% of the mean observed ET in the Southern Great plains-USA.

Keywords: evapotranspiration, remote sensing, SWIR

1. Introduction

Many hydrologic and global circulation models as well as agricultural systems require estimates of ET for a wide range of the surface conditions and spatial-temporal scales (Venturini et al., 2008). The ET is the most significant withdrawal of water in the water balance, so that its calculation represents a real challenge to water resources practitioners. Indeed, during the last decades, the scientific community has been concerned about errors in ET estimates and measurements. The advent of satellite technology implied a significant

advance for the scientific community, which made possible the derivation of new methodologies to estimate ET from remotely sensed data. Three categories of ET models can exemplify the scientific advance in this topic (Courault et al., 2005). The empirical and semi-empirical methods, as for example the models proposed by Priestley and Taylor (1972), Granger and Gray (1989), Carlson et al. (1995), Jiang and Islam (2001), Rivas and Caselles (2004), among others, use site specific or semi-empirical relationships between two or more variables. The Residual methods calculate the energy budged and ET as the residual of the energy balance. The Surface Energy Balance Algorithm for Land (SEBAL) (Bastiaanssen, 2000) is within this category. Finally, the indirect methods involves Soil-Vegetation-Atmosphere Transfer (SVAT) models with physically based methods, that present different levels of complexity often reflected in the number of parameters. The ISBA (Interactions between Soil, Biosphere and Atmosphere) model published by Noilhan and Planton (1989) is an example of this category.

Nowadays, space-born sensors are crucial data sources for any of the models within the three categories. Not only for their efficiency in monitoring different terrestrial ecosystems but also for the type and quality of the information delivered. Commonly, networks of meteorological stations represent the main source of atmospheric data while information about the surface was obtained from space-born sensors (Price, 1990; Gillies et al., 1997). However, after launching MODIS sensors, atmospheric data are also available from satellite remote sensors. Empirical and semi-empirical ET models had proliferated with the availability of thermal infrared images (Jiang and Islam, 2001; Rivas and Caselles, 2004; Venturini et al., 2008; Anderson et al., 2011a; Long and Singh, 2012; Gokmen et al., 2012). Venturini et al., (2008) presented a new formulation to derive ET maps from remotely sensed data without auxiliary relationships or site-specific relationships. The formulation is based on Granger's complementary relationship and Priestley–Taylor's equation (P-T from now on). The model eliminates the need of computing the wind function and resistance parameters, by including the relative evaporation parameter. By combining the relative evaporation parameter, Granger's complementary relationship and P-T equation, the authors obtained a simple equation to estimate ET. Venturini et al. equation requires the calculation of T_u, which originally was obtained from an inefficient method (Venturini et al., 2011).

Hence in this paper we propose a simple methodology that relates T_u to the surface moisture availability concept defined by Barton (1979). For this, we made use the water absorption properties of SWIR bands. This property was widely used to derive surface water content. For instance, Hunt and Rock, (1989) showed that the water content in the vegetation is clearly related to the reflectance in the SWIR wavelengths, between 1100 and 2500 nm. Cecatto et al., (2002a) demonstrated that over 50% of the changes in reflectance of the SWIR bands are due to the absorption caused by the water content in the vegetation. Regardless of the absorption of the plant pigment, the water absorption influences the reflectance of the NIR and SWIR (Cheng et al., 2008). Combinations of near infrared (NIR) and SWIR has been used to study the plant water content (Hunt et al., 1987, Gao, 1996, Peñuelas et al., 1997, Ceccato et al., 2001, Chen et al., 2005).

Consequently, we propose a surface moisture indicator from the SWIR reflectance that would yield a better T_u estimation, assuming the reflectance of a given pixel is the aggregated response of different types of surfaces. Thus, T_u would only depend on the surface characteristics. This new T_u computation greatly improves the original Venturini model, as it will be shown in section 4.

2. Venturini et al. method

Venturini et al., (2008), V-V from now on, modified the P-T model using the Granger`s complementary relationship (Granger, 1989*)* and the relative evaporation, defined as the ratio between ET and potential evapotranspiration (E_{pot}). The relative evaporation proposed by Granger and Gray (1989) was used to define a coefficient F assuming that the wind speed function similarly affects ET and E_{pot}. The authors also assumed that the saturation and actual vapor pressures can be calculated from the saturation vapor pressure curve (SVP) (Figure 1), with temperature data. Thus, F=ET/E_{pot} can be expressed as (Venturini et al., 2008),

$$F = \frac{ET}{E_{pot}} = \frac{(e_s - e_a)}{(e_s^* - e_a)} \cong \frac{(T_u - T_d)\Delta_1}{(T_s - T_d)\Delta_2} \quad (1)$$

where e_s is the surface actual vapor pressure, e^*_s is the surface saturation vapor pressure, e_a is the air actual vapor pressure, T_s is the surface temperature, T_u is the temperature of the

surface if it is brought to saturation without changing the actual surface vapor pressure, which in turn is analogous to the dew point temperature (T_d) definition.

Accordingly, E_{pot}= ET/F (see equation 1) combined with Granger´s equation, renders ET as a function of wet environment evapotranspiration (E_w),

$$ET + \frac{ET\gamma}{F\Delta} = E_w\left(\frac{\gamma + \Delta}{\Delta}\right) \quad (2)$$

where γ is the psychrometric constant, Δ is the slope of the SVP curve and E_w is wet environment evapotranspiration.

Then, P-T equation was used to compute E_w. Consequently, combining P-T expression with equations (2) and (1), the following model was derived,

$$ET = \alpha\left(\frac{F\Delta}{F\Delta + \gamma}\right)(R_n - G) \quad (3)$$

where, α is a Priestley and Taylor's parameter and for saturated surfaces α is typically assumed to be equal to 1.26, R_n is the net radiation and G is soil heat flux.

The new variable, T_u, introduced in this formulation, is needed to determine e_s and then F. The authors determined T_u from the SVP curve as a surrogate of e_s, however they recognize the limitation of this method. A full discussion regarding the definition of T_u and its calculation can be found in Venturini et al., (2008) and Venturini et al., (2011).

Once T_u is estimated, it is possible to compute e_s then F and ET.

2.1 A new formulation to estimate e_s

The e_s estimation is improved by using of surface variable, such as the surface moisture (SM). The new e_s calculation involves the surface water availability (Barton, 1979), that is estimated as,

$$\sigma = \frac{e_S}{e^*_S} \quad (5)$$

where σ is a measure of the surface moisture availability (Barton, 1979).

Considering that the SWIR energy is absorbed by the water and therefore these bands are sensitive to the surface moisture content variations (Chen et al., 2005), for practical purposes σ is estimated from the SWIR reflectance (at 1300 – 2500 nm) and related to the concept of relative humidity of an evaporating surface.

The SWIR bands have been used to derive water content of vegetation and soil moisture (Knaeps et al., 2012). Many authors combined NIR and SWIR reflectance to study changes in foliar water content (Hunt et al., 1987, Gao, 1996; Peñuelas et al., 1997; Ceccato et al., 2001; Fensholt and Sandholt, 2003; Sims and Gamon, 2003; Zarco-Tejada et al., 2003; Maki et al., 2004; Chen et al., 2005; Cheng et al., 2006; Trombetti et al., 2008). There are others parameters that affect the vegetation SWIR reflectance, for instance the leaf/surface internal structure and dry matter content, but they are negligible compared with water absorption (Fensholt and Sandholt, 2003). Over 50 % of the changes in reflectance of the SWIR bands are due to the absorption caused by the water content in the vegetation (Cecatto et al., 2002a).

The strong water absorption occurring at wavelengths > 1.0 μm, makes the surface moisture the main cause of the reflectances variation. Thus, in the SWIR, the dry soils have higher reflectance than wet soils (Lovell and Asner, 2002). In addition, the reflectance in the SWIR is negatively related to the water content of the vegetation (Yilmaz et al., 2008). Therefore, considering the surface as a vegetation-soil complex and assuming that the decrease of the reflectance in the SWIR is essentially due to the water content of the surface, we can approximate σ as,

$$\sigma = \frac{\text{Rsat}}{\text{Ri}} \tag{6}$$

where Rsat is the reflectance of a saturated surface and Ri is the SWIR reflectance of i pixel.

In this method, Rsat is easily obtainable from the relationship between Ri and soil moisture (SM), if ground data are available, otherwise it can be calculated from the mean Ri of those pixels identified as water in a image. In any case, values of Ri close to zero represent saturated pixels and can be taken as Rsat.

Then, e_s is estimated as σe^*_s (see equation 5) and it is introduced in equation 1 to compute F, to finally apply equation 3 to estimate ET. This modified form of the Venturini model will refer hereinafter as G-V.

3. Competitive ET equations to contrast the new ET methodology

Several ET models and methods originated from equations such as those proposed by Penman (1948) and Priestley and Taylor (1972). These authors provided two remarkable methodologies that support many of the ET models available today, whether they strive on energy fluxes estimation or water vapor mass transport.

The P-T physically based model stands for its simplicity and data requirements. The original equation was developed for saturated surfaces assuming that the advective processes are negligible, so it does not include the terms and resistance factors. Under these assumptions the authors derived the following equation for calculating ET from a saturated surface:

$$\lambda E = \alpha \left[\frac{\Delta}{(\Delta + \gamma)} \right] (Rn - G) \tag{7}$$

where α is the P-T coefficient. α value was obtained empirically and the authors determined that varies between 1.26 and 1.28, but the value accepted by the scientific community is 1.26.

Jiang and Islam (2001), from now on refers to as J-I, modified P-T equation for heterogeneous unsaturated surfaces. Their approach was based on an interpretation of the Triangle Method (Gillies and Carlson, 1995), so-called because of the triangular distribution of pixels customarily observed when the data is plotted in the T_s *versus* NDVI space. J-I interpreted that the pixels along the warm edge represent the minimum ET for each vegetation class, while the cold edge bounds the maximum ET, thus the actual magnitude of ET can vary within these bounds. Further, a coefficient ϕ was estimated by a simple two-step linear interpolation between the sides of the triangle. This coefficient links physical characteristics of the pixels with ET.

The original V-V ET equation, as well as the G-V method also modified the P-T equation, thus it is reasonable to contrast G-V results with V-V, J-I and P-T estimates. For clarity, the equations derived for these authors are summarized in Table 1.

4. Study Area and Data

4.1 Study Area

The SGP region extends over the State of Oklahoma and southern part of Kansas, running from longitude 95.5º W to 99.5º W and from latitude 34.5º N to 38.5º N. It has flat terrain,

with heterogeneous land cover and a wide variety of weather through the year. Winters are very cold and summers are very hot and humid. The prairies support an abundant wildlife in undisturbed settings.

This region has relatively extensive and well distributed coverage of ground Energy Fluxes and Bowen stations, maintained by the Atmospheric Radiation Measurement (ARM) program (http://www.arm.gov). The stations are widely distributed over the whole domain (Figure 1). The sites are named according to the instruments located in each facility and numbered sequentially as each new center is open. e.g. "E5" refers to extended facility sites number 5. Extended facility instruments include an Energy Balance Bowen Ratio system (EBBR), which produces 30 minute estimates of the vertical fluxes of sensible and latent heat at the local surface.

The data from the following stations had been used in this work; station E8 and E22 are localized in a grazed rangeland region, E4 is in an ungrazed rangeland area, E13 is positioned in a region with pasture and wheat, E7, E9, E15, E20 and E27 are located in pastures. E18 and E19 are in ungrazed pasture area, E12 is located in a native prairie, E10 is in alfalfa, E16 is in wheat region and E2 is in grass region.

3.2 Data and image

The fluxes from the EBBR stations are calculated from observations of net radiation, soil surface heat flux, and the vertical gradients of temperature and relative humidity (RH).

The R_n, G and air pressure data collected by the EBBR were used to estimate ET with the methods presented in Table 1. The latent heat flux data was used in the validation of G-V methodology.

The imageries used in this work were provided by MODIS sensor. MODIS is one of the instruments on board EOS-Terra and EOS-Aqua satellites http://modis.gsfc.nasa.gov/ (Justice et al., 2002; Vermote et al., 2002). Daytime MODIS-Aqua images for nine days in years 2009, 2010 and 2011 during Spring and Summer, with at least 80% of the study area free of clouds were selected. Table 2 summarizes the image information including date, day of the year, satellite overpass time and image quality. MYD02, MYD07 and MYD11 were the three products needed for this application. The MYD02 has corrected radiance, reflectance and geolocations for 36 bands at 1x1 km. The MODIS Atmospheric profile

(MOD07) offers several parameters, of which air and dew point temperature profiles were used in the current study. The spatial resolution of this daily product is 5×5 km^2, at 20 vertical atmospheric pressure levels (Menzel et al., 2002). The MYD11 product supplies T_s images on a daily base (Wan and Dozier, 1996; Venturini et al., 2004; Venturini et al., 2011).

4-Results

4.1 Preprocessing

The MODIS images were georeferenced from the geographical coordinates (Latitude and Longitude) provided in each product. The air and dewpoint temperatures, required to calculate the vapor pressure deficits, corresponded to the vertical pressure level of 950 hPa, close to the surface. It is worthy to note, that the temperatures are assumed to be homogenous over the 5×5 km (Menzel et al., 2002). The study area was pulled out of each image and geographically projected in a grid of 445 columns by 445 rows, in pixels of approximately 1 km resolution.

The reflectance of the red band (R), NIR and SWIR band 7 (R7) were corrected by atmospheric effects following the dark object method (Chavez, 1996). The R and NIR images are used to estimate the NDVI with the following expression:

$$NDVI = \frac{NIR - R}{NIR + R} \tag{8}$$

With R7 images, σ was approximated. The T_s and T_d images were used to estimate, e^*_s and e_a with Buck´s equation (Buck, 1981). Finally, we applied the equations of Table 1 and we compared the results.

4.2 Analysis of σ

To obtain sigma σ equation 6, it is necessary to know Rsat. In this case, Rsat was obtained from the R7 *versus* soil moisture (SM) data, expressed in gravimetric percentage (Figure 2(a)). The EBBR-SM data at 5 cm were selected because they are the nearest to the surface. Figure 2 (a) shows that the R7 became asymptotic at 0.06 for SM values greater than 25 %, indicating the limit of the surface saturation condition (Hillel, 1998). This value is consistent to the regional water reflectance (RWR) in the SWIR band obtained as

$RWR=(\sum R_d^{water})/n$, where R_d^{water} is the reflectance mean of the pixels identified as water (NDVI <0) in the SWIR band on a given day, and n is the total of days analyzed. Then, σ was obtained for each of the days tested and the regional statistic (means, minimums and maximums and standard deviation) are shown in Table 3. The maximum σ value is approximately equal to 1 on all days studied, suggesting that there were saturated pixels during the studied period. The minimum σ value varies from 0.14 to 0.22, showing that there may be pixels with low SM. The reflectance in the SWIR, in general, is not greater than 0.6 for this region and during the studied seasons. The σ regional means values vary between 0.37 and 0.59 and standard deviations from 0,076 to 0,178, consistent with different degree of dispersion around the mean.

In order to analyze the σ sensitivity to capture different moisture conditions, it is contrasted with SM. Thus, σ *vs* SM were plotted. The relationship yielded a determination coefficient (R^2) of 0.68. Figure 2 (b) displays the relationship between σ and SM. Assuming that SM values >25% would be the limit of the surface saturation condition, σ values greater than 0.70 indicate a saturated surface. Barton (1979) found that for bare soil surface σ ≈1 for surface moisture contents >35% on a dry soil weight. Day 04/05/2011 was selected to exemplify the general regional variations because it presented only 1% of cloud cover. Finally, Figure 2 (c) shows the areal distribution of SM and σ for the day 04/05/2011, where a good general agreement is observed. Station E19 was selected because it was available in the 80% of the days analyzed. Figure 2 (d) displays a temporal variation of SM and σ for station E19. Both variables (σ and SM) seems to follow the same variation over time, although the SM field data scale is punctual and σ is the response of a mixed pixel of 1 km^2 approximately.

4.3 Validation of ET

The observed ET (ET_{ground}) was contrasted with ET estimates from those methods in Table 1 ($ET_{calculates}$) in 54 samples. The regional maximum, minimum and average ET values are shown in Table 4. It can be observe that J-I, V-V and G-V methods yielded similar results, all of them lower than those obtained by P-T model. I should be kept in mind that P-T's model represents E_w concept, while J-I, V-V and G-V methods represent the actual ET, (Venturini et al., 2008). The mean ET ground data differs from the mean ET models in

28.24 Wm^{-2}, 13.10 Wm^{-2} and -14.69 Wm^{-2} for J-I, V-V and G-V respectively. These differences are comparable to those presented by other authors (Kustas et al., 2003; Batra et al., 2006; Venturini et al., 2008). While J-I and V-V overestimate the ET, the G-V model would underestimate regional ET.

The statistic used to analyze the goodness of the new model is the Bias, the root mean square error (RMSE) and correlation coefficient (r). The Bias was calculated as $(ET_{ground}-ET_{calculates})/n_{obs}$ and the RMSE as $((ET_{ground}-ET_{calculates})^2/n_{obs})^{0.5}$, where n_{obs} is the number of observations (54 points). The J-I and V-V methods presented similar over all RMSE which is the 19 % of observed ET. The Bias was of 8% for J-I method and 4% for V-V model. The G-V methodology yield RMSE of 39.92 Wm^{-2} and -14.69 Wm^{-2} for Bias, which represent 11% and 4% of the observed mean ET, respectively. The r values were 0.92, 0.74 and 0.82 for G-V, V-V and J-I methods respectively; while the P-T method presented a r=0.54. These preliminary results suggest that G-V model correlate better with the measurements than the others models contrasted here. Figure 3 shows the contrast between calculated and observed ET. Results from J-I and V-V models do not present significant difference. Both models tend to overestimate the ET. Results with P-T model are larger than the others, accordingly with E_w concept. The G-V model present a good fit to the observed ET.

Our literature review indicates that G-V models would imply an important improvement in ET estimates with remotely sensed data. For instance, Venturini et al., (2008) published values of RMSE and bias of the order of 18% and 15% of the observed mean ET for the same region. Kalma et al., (2008) conducted a thorough analysis where results from about 30 published ET validation studies were summarized. These authors reported RMSE values of about 50Wm^{-2} and relative errors of about 15 to 30%. Long and Singh, (2012) recently published RMSE of 45.6 Wm^{-2} and 63.1 Wm^{-2} using Landsat TM/ETM+ and ASTER images, respectively.

Table 5 shows the RMSE and bias for each analyzed day for J-I, V-V and G-V models. In general, the RMSEs for G-V model are less than 13% of the mean values for each day; the biases are lower than 8% of the observed mean ET. Only the day 04/06/2010 presented a RMSE of 18% with a Bias of the same order. The quality of the day 04/06/2010 image is not very good and few stations are free of clouds, which may cause uncertainties in the

imagery. The V-V and J-I methods present similar errors for the data set analyzed here, reaching RMSE maximum values of approximately 30% of the observed ET mean.

Clearly, T_u obtained from σ improvement the V-V model results. The T_u, as defined by Venturini et al. (2008), is a parameter that describes the surface moisture state. The σ incorporated in G-V methodology represents the state of the surface moisture consistent to T_u and e_s definition.

The selection of the best method would be based on the available data and simplicity of programming a routinely application. The new G-V method seems to improve ET estimates and it is simple to obtain with remotely sensed data. J-I method yielded larger errors and the NDVI-Ts plot needs supervision to ensure the triangular shape. V-V method as well as G-V method can be coded and routinely applied without supervision.

5- Discussion

The ET calculation has been a challenge for hydrologists and water managers. ET is the most significant withdrawal of water in any ecosystem, reason why its estimation requires precise methods.

In general, many of the current ET models require little amount of ancillary ground data (Jiang and Islam, 2001; Nishida et al., 2003; Venturini et al., 2008). Nowadays, space-born sensors are crucial data sources for any of empirical o physically based models; not only for their efficiency in monitoring different terrestrial ecosystems but also for the type and quality of the information delivered.

In this work, Venturini et al. methodology was modified to improve the estimation of the main parameter of their method. Venturini et al. (2008) model requires the knowledge of the T_u parameter, which was originally obtained from the surface actual water vapor pressure curve. Here, a simple methodology that relates e_s to the reflectance of the surface in the SWIR bands is proposed. The new formulation relates the SWIR properties to the Barton´s σ parameters, that was defined as e_s/e^*_s. Thus, we proposed to obtain σ as the ration between the SWIR reflectance of the water and the common pixel reflectance. This estimation of σ was analyzed against SM data to verify that it really represent the moisture content of each pixel. Our analysis showed that σ follows the spatial and temporal variation of SM data. It should be note that Rsat, i.e. the water reflectance in the SWIR bands, can be

estimated with the information in the image or with ground data of SM. Our analysis of this two option suggested that ET results are similar. In other words, both forms of Rsat yield similar values.

In order to verify the goodness of the new ET estimates, they were compared with the original Venturini et al.'s method, P-T result and J-I estimates. Besides, the results of these ET models were contrasted with observed ET as presented in session 4. Ground data are overestimated by J-I and V-V results, with RMSEs of about 60 W/m^2 (19% of observed ET). The G-V method yield smaller RMSE and bias (11% and 4 % respectively).

Although this comparison is no exhausted, ET results with G-V methodology are better than competitive models in all the days (see Table 5). J-I and V-V models, overestimate the observed data in less than 8% with an averaged error smaller than 20 % of the mean observed ET. The G-V estimates would underestimate ET in less than 4% with an averaged error of the 11% of the mean observed ET.

The selection of the best model depends on the data availability, the type of application and end users expertise. In this regard, the new methodology to obtain T_u improves ET results with a simple and easy to apply σ parameter. The combination of V-V original model and the new parameter lead to a more accurate and robust model that would largely help to decision makers.

6- References

Anderson, M. C., Hain, C. R., Wardlow, B., Mecikalski, J. R., Kustas, W. P. (2011a). Evaluation of a drought index based on thermal remote sensing of evapotranspiration over the continental U.S. *Journal of Climate*, 24, 2025–2044.

Barton, I. J. (1979). A parameterization of the evaporation from nonsatured surfaces. surfaces. *Journal of Applied Meteorology*, 18, 43-47.

Batra, N., Islam, S., Venturini, V., Bisht, G., Jiang, L. (2006). Estimation and Comparison of Evapotranspiration from MODIS and AVHRR sensors for Clear Sky Days over the southern Great Plains. *Remote Sensing of Environment*, 103, 1-15.

Bastiaanssen, W.G.M. (2000). SEBAL-based sensible and latent heat fluxes in the irrigated Gediz Basin, Turkey. *Journal of Hydrology*, 229, pp. 87-100, ISSN 0022-1694.

Buck, A.L. (1981). New equations for computing vapor pressure and enhancement factor. *Journal of Applied Meteorology,* 20, pp. 1527-1532.

Carlson, T. N., Gillies, R. R., Schmugge, T. J., (1995). An interpretation of methodologies for indirect measurement of soil water content. *Agricultural and Forest Meteorology*. 77, 191-205.

Ceccato, P., Flasse, S., Tarantola, S., Jacquemoud, S., Gregoire, J. M. (2001). Detecting vegetation leaf water content using reflectance in the optical domain. *Remote Sensing of Environment*, 77, pp. 22– 33.

Ceccato, P., Gobron, N., Flasse, S., Pinty, B., Tarantola, S. (2002a). Designing a spectral index to estimate vegetation water content from remote sensing data: Part 1. Theoretical approach. *Remote Sensing of Environment*, 82, pp.188– 197.

Chavez, P. (1996). Image based atmospheric corrections-revisited and improved. *Photogrammetric Engineering and Remote Sen*sing 62: 1025-1036.

Chen, D., Huang, J., Jackson, T. (2005). Vegetation water content estimation for corn and soybeans using spectral indices derived from MODIS near- and short-wave infrared bands. *Remote Sensing of Environment* 98, pp. 225 – 236

Cheng, Y., Ustin, S., Riaño,D., Vanderbilt, V. (2008). Water content estimation from hyperspectral images and MODIS indexes in Southeastern Arizona. *Remote Sensing of Environment*, 112, pp. 363–374

Cheng, Y. -B., Zarco-Tejada, P. J., Riano, D., Rueda, C. A., Ustin, S. L. (2006). Estimating vegetation water content with hyperspectral data for different canopy scenarios: Relationships between AVIRIS and MODIS indexes. *Remote Sensing of Environment*, 105, 354−366.

Courault, D., Seguin, B., Olioso, A. (2005). Review to estimate Evapotranspiration from remote sensing data: Some examples from the simplified relationship to the use of mesoscale atmospheric models. *Irrigation and Drainage Systems,* 19,223-249, ISSN 0168-6291.

Fensholt, R. and Sandholt, I. (2003). Derivation of a shortwave infrared water stress index from MODIS near- and shortwave infrared data in a semiarid environment. *Remote Sensing of Environment*, 87, pp. 111−121.

Gao, B. C. (1996). NDWI—A normalized difference water index for remote sensing of vegetation liquid water from space. *Remote Sensing of Environment*, pp. 58, 257–266.

Gillies, R.R. and Carlson T.N. (1995). Thermal remote sensing of surface soil water content with partial vegetation cover for incorporation into mesoscale prediction models. J. *Appl. Meteorol*., 34, pp. 745–756

Gillies, R.R., Carlson,T.N., Cui, J., Kustas, W.P., Humes, K.S. (1997). A verification of the 'triangle' method for obtaining surface fluxes from remote measurements of the Normalized Difference Vegetation Index (NDVI) and surface radiant temperature. *International Journal of Remote Sensing, 18*(15), 3145-3166.

Gokmen M., Vekerdy Z., Verhoef A., Verhoef W., Batelaan O., Van Der Tol C. (2012). Integration of soil moisture in SEBS for improving evapotranspiration estimation under water stress conditions. *Remote Sensing of Environment* 121, 261–274

Granger, R.J. (1989). A complementary relationship approach for evaporation from nonsaturated surfaces. *Journal of Hydrology*, 111, pp. 31-38, ISSN 0022-1694

Granger, R.J. and Gray, D.M. (1989). Evaporation from natural nonsaturated surfaces. *Journal of Hydrology,* 111, pp. 21-29, ISSN 0022-1694.

Hunt Jr., E. R. and Rock, R. N. (1989). Detection of changes in leaf water content using near- and middle-infrared reflectance. *Remote Sensing of Environment*, 30, pp. 43–54.

Hunt, E. R., Rock, B. N., Nobel, P. S. (1987). Measurement of leaf relative water content by infrared reflectance. *Remote Sensing of Environment*, 22, pp. 429– 435.

Hillel, D. (1998). ENVIRONMENTAL SOIL PHYSICS. Academic Press. Amsterdan. 771 pags.

Jiang, L. and Islam, S. (2001). Estimation of surface evaporation map over southern Great Plains using remote sensing data. *Water Resources Research*, *37*(2), 329-340. ISSN 0043-1397.

Justice CO, Townshend JRG, Vermote EF, Masuoka E, Wolfe RE, Saleous N, Roy DP, Morisette JT. (2002). An overview of MODIS Land data processing and product status. *Remote Sensing of Environment*, *83(2-Jan),* pp. 3-15.

Kalma, J. D., McVicar T. R., McCabe, M. F. (2008). Estimating Land Surface Evaporation: A Review of Methods Using Remotely Sensed Surface Temperature Data. *Surveys in Geophysics*. Volume 29, Numbers 4-5, 421-469

Knaeps E., Dogliotti A.I., Raymaekers D., Ruddick K., Sterckx S. (2012). In situ evidence of non-zero reflectance in the OLCI 1020 nm band for a turbid estuary. *Remote Sensing of Environment* 120, 133–144

Kustas, W. P., Norman, J. M., Anderson, M. C., French, A. N. (2003). Estimating sub-pixel surface temperature and energy fluxes from the vegetation index-radiometric temperature relationship. *Remote Sensing of Environment*, 85, 429–440.

Long D. and Singh V. P. (2012). A Two-source Trapezoid Model for Evapotranspiration (TTME) from satellite imagery. *Remote Sensing of Environment* 121, 370–388.

Lobell, D.B. and Asner, G.P. (2002). Moisture effects on soil reflectance. *Soil Science Society of America Journal*, 66 pp. 722–727

Maki, M., Ishiahra, M., Tamura, M. (2004). Estimation of leaf water status to monitor the risk of forest fires by using remotely sensed data. *Remote Sensing of Environment*. 90:441-450.

Menzel, W.P., Seemann, S.W., Li, J., Gumley, L.E. (2002). MODIS Atmospheric Profile Retrieval Algorithm Theoretical Basis Document, Version 6, Reference Number: ATBD-MOD-07. http://modis.gsfc.nasa.gov/ data/atbd/atbd_mod07.pdf (accessed on 12/04/2003).

Nishida, K., Nemani, R.R., Running, S.W., Glassy, J.M. (2003). An operational remote sensing algorithm of land evaporation. *Journal of Geophysical Research*, 108, D9, 4270, doi:10.1029/2002JD002062, ISSN 0148-0227.

Noilhan, J. and Planton, S. (1989). GCM gridscale evaporation from mesoscale modelling. *Journal of Climate,* 8, pp. 206-223, ISSN 0894-8755

Penman, H.L. (1948). Natural evaporation from open water bare soil and grass. Proceedings of the Royal Society of London. Series A Mathematical and Physical Sciences 193 (1032), 120–145.

Peñuelas, J., Piñol, J., Ogaya, R., Filella, I. (1997). Estimation of plant water concentration by the reflectance water index (R900/R970). *International Journal of Remote Sensing,* 18, pp. 2869–2875.

Price, J.C. (1990). Using spatial context in satellite data to infer regional scale evapotranspiration. *IEEE Transactions on Geoscience and Remote Sensing*, 28, 5, pp. 940-948, ISSN 0196-2892

Priestley, C.H.B. and Taylor, R.J. (1972). On the Assessment of Surface Heat Flux and Evaporation Using Large-Scale Parameters. *Monthly Weather Review,* 100, pp. 81–92, **ISSN** 0027-0644.

Rivas, R. and Caselles, V. (2004). A simplified equation to estimate spatial reference evaporation from remote sensing-based surface temperature and local meteorological data. *Remote Sensing of Environment*, 83, pp. 68-76, ISSN 0034-4257.

Sims D.A. and Gamon J.A. (2003) Estimation of vegetation water content and photosynthetic tissue area from spectral reflectance: a comparison of indices based on liquid water and chlorophyll absorption. *Remote Sensing of Environment.* 84:526-537.

Trombetti, M., Riano, D., Rubio, M. A., Cheng, Y. B., Ustin, S. L. (2008). Multi-temporal vegetation canopy water content retrieval and interpretation using artificial neural networks for the continental USA. *Remote Sensing of Environment*, 112: 203-215.

Venturini, V., Bisht, G., Islam, S., Jiang, L. (2004). Comparison of evaporative fractions estimated from AVHRR and MODIS sensors over South Florida. *Remote Sensing of Environment*, *93*, 77-86.

Venturini, V., Islam, S., Rodríguez, L., (2008). Estimation of evaporative fraction and evapotranspiration from MODIS products using a complementary based model. R*emote Sensing of Environment.* 112, pp. 132-141, ISSN 0034-4257.

Venturini, V., Rodríguez, L., Bisht, G. (2011). A comparison among different modified Priestley and Taylor's equations to calculate actual evapotranspiration with MODIS data. *International Journal of Remote Sensing*. 32, 1319–1338.

Vermote, E.F., Saleous, N.Z., Justice, C.O. (2002). Atmospheric correction of MODIS data in the visible to middle infrared: first results. *Remote Sensing of Environment*, *83(2-Jan),*pp. 97-111.

Wan, Z. and Dozier, J.A. (1996). A generalized split-window algorithm for retrieving land-surface temperature from space. IEEE *Transactions on Geoscience and Remote Sensing, 34(4),* 892–905.

Yilmaz, M.T., Hunt Jr. E.R., Goins, L.D., Ustin, S.L., Vanderbilt, V.C., Jackson T.J. (2008). Vegetation watercontent during SMEX04 from ground data and Landsat 5 Thematic Mapper imagery. *Remote Sensing of Environm*ent, 112, pp. 350–362.

Zarco-Tejada, P. J., Rueda, C. A., Ustin, S. L. (2003). Water content estimation in vegetation with MODIS reflectance data and model inversion methods. *Remote Sensing of Environment*, 85, 109–124.

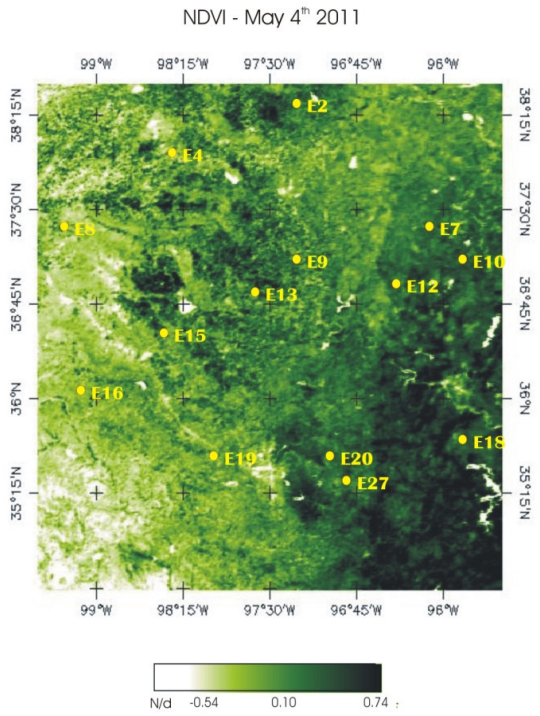

Figure 1: Southern Great Plains and ground station locations.

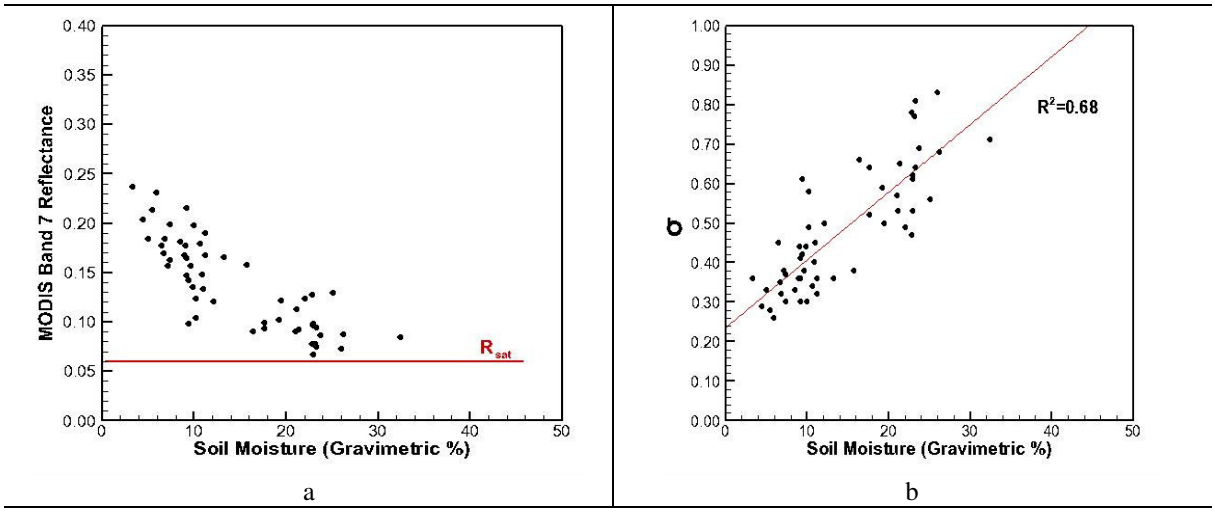

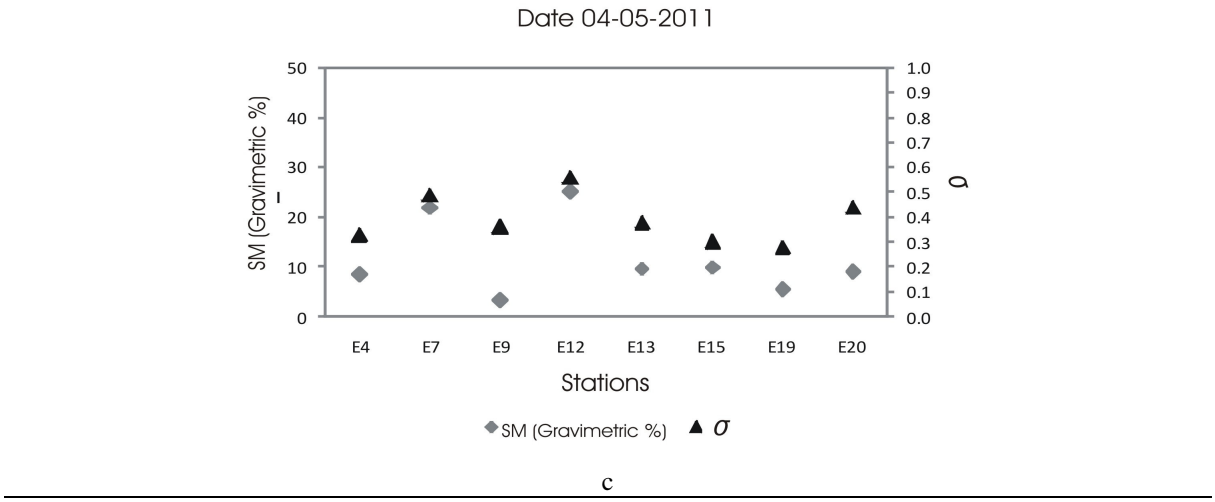

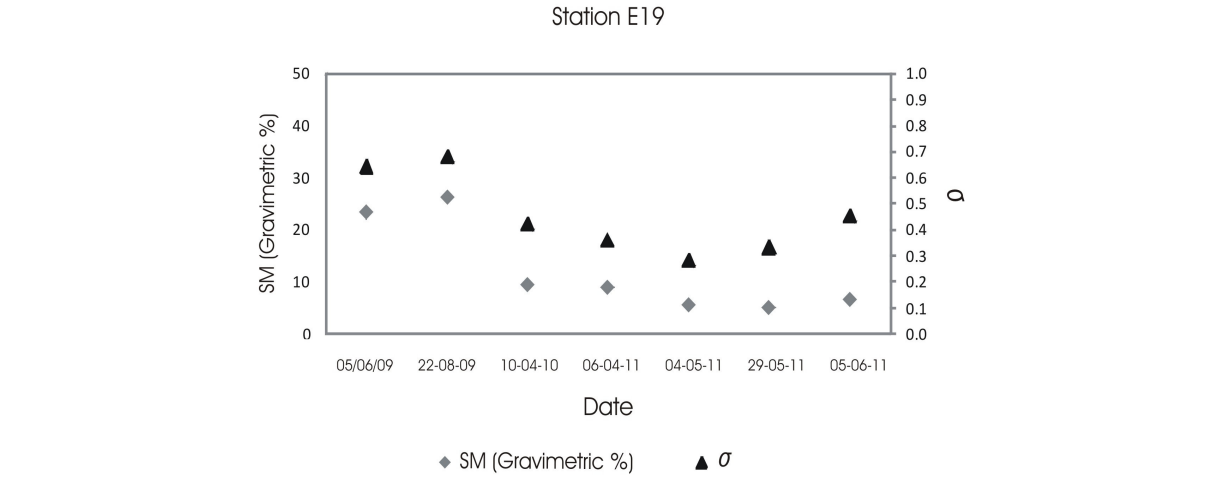

Figure 2: (a) R_i vs SM relationship and overlay R_{sat}; (b) σ vs SM; (c) σ vs SM for day 04/05/2011 and (d) σ vs SM for station E19

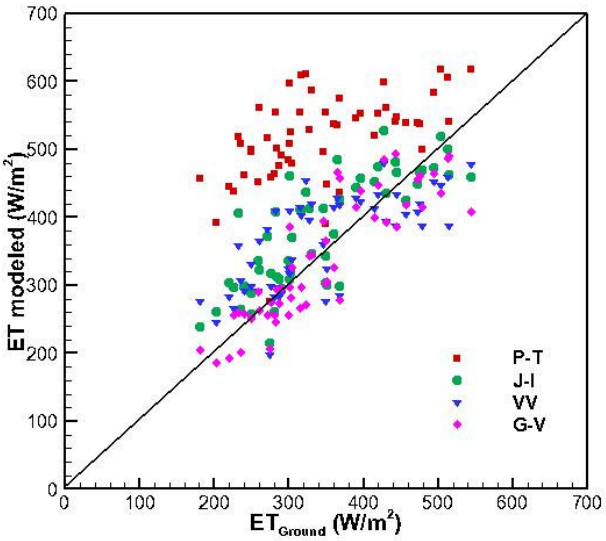

Figura 3: ET ground observations vs estimates ET

Table 1: Summary of different methods to obtain ET

Author	Equation	Main parameter
Priestley and Taylor (1972) (P-T)	$\mathrm{Ew} = \alpha\left[\frac{\Delta}{\Delta+\gamma}\right](\mathrm{R_n} - \mathrm{G})$	α
Jiang and Islam (1999) (J-I)	$\mathrm{ET} = \phi\left[\frac{\Delta}{\Delta+\gamma}\right](\mathrm{R_n} - \mathrm{G})$	ϕ
Venturini et al. (2008) (V-V)	$\mathrm{ET} = \alpha\left(\frac{\mathrm{F}\Delta}{\mathrm{F}\Delta+\gamma}\right)(\mathrm{R_n} - \mathrm{G})$	F(T_u)
Girolimetto and Venturini (G-V)	$\mathrm{ET} = \alpha\left(\frac{\mathrm{F}\Delta}{\mathrm{F}\Delta+\gamma}\right)(\mathrm{R_n} - \mathrm{G})$	F(σ)

Table 2: Date, day of the year, overpass time and image quality of the nine study days

Date	Day of the year (DOY)	Overpass time (UTC)	Image quality (% clouds)
April 6th 2011	96	19:30	15
May 4th 2011	124	19:55	1
May 26th 2011	146	19:20	2
May 29th 2011	149	19:50	1
June 5th 2011	156	19:55	14
April 10th 2010	100	19:40	5
June 4th 2010	155	19:45	18
June 5th 2009	156	19:25	14
August 22th 2009	234	19:35	11

Table 3: Regional statistics of σ

Date	Max	Min	Mean	Standard deviation
April 6th 2011	0.99	0.15	0.40	0.077
May 4th 2011	0.99	0.16	0.37	0.098
May 26th 2011	0.99	0.20	0.55	0.178
May 29th 2011	0.99	0.16	0.40	0.132
June 5th 2011	0.99	0.14	0.38	0.140
April 10th 2010	0.99	0.17	0.41	0.076
June 4th 2010	0.99	0.17	0.44	0.112
June 5th 2009	0.99	0.22	0.58	0.150
August 22th 2009	0.99	0.18	0.59	0.171

Table 4: General static of calculated ET and ET_{ground} for 54 point sample at the pixel scale

ET model	Max	Min	Mean
ET_{ground}	544.63	180.18	350.62
P-T	617.19	275.15	517.11
J-I	526.65	214.55	378.86
VV	478.97	196.63	363.72
G-V	492.91	185.48	335.93

Tabla 5: ET (W/m 2) comparison between observations and proposed method estimates for each day analyzed.

Date	# of observations	J-I method		VV method		G-V method	
		RMSE	Bias	RMSE	Bias	RMSE	Bias
April 6th 2011	6	110.24	79.83	96.52	28.74	44.34	23.07
May 4th 2011	6	91.77	79.77	98.84	70.95	36.03	-23.83
May 26th 2011	4	39.08	30.24	20.95	10.84	16.97	7.01
May 29th 2011	6	47.92	-10.38	70.63	3.54	39.15	-23.77
June 5th 2011	8	37.78	8.66	55.42	24.16	36.78	-18.82
April 10th 2010	5	64.89	62.71	44.67	42.42	29.63	-8.75
June 4th 2010	4	45.69	-9.06	51.69	-19.97	84.05	-74.97
June 5th 2009	8	37.61	-5.32	65.95	-24.67	31.53	-19.95
August 22th 2009	7	36.53	29.18	34.24	-11.94	25.85	-2.92